

FEDSM-ICNMM2010-31032

THE BALANCED-FORCE VOLUME TRACKING ALGORITHM AND GLOBAL EMBEDDED INTERFACE FORMULATION FOR DROPLET DYNAMICS WITH MASS TRANSFER¹

LA-UR-10-02034

Marianne M. Francois

Computational Physics and Methods group
Los Alamos National Laboratory
Los Alamos, NM 87545, USA

Neil N. Carlson

Computational Physics and Methods group
Los Alamos National Laboratory
Los Alamos, NM 87545, USA

ABSTRACT

Understanding the complex interaction of droplet dynamics with mass transfer and chemical reactions is of fundamental importance in liquid-liquid extraction. High-fidelity numerical simulation of droplet dynamics with interfacial mass transfer is particularly challenging because the position of the interface between the fluids and the interface physics need to be predicted as part of the solution of the flow equations. In addition, the discontinuity in fluid density, viscosity and species concentration at the interface present additional numerical challenges. In this work, we extend our balanced-force volume-tracking algorithm for modeling surface tension force (Francois et al., 2006) and we propose a global embedded interface formulation to model the interfacial conditions of an interface in thermodynamic equilibrium. To validate our formulation, we perform simulations of pure diffusion problems in one- and two-dimensions. Then we present two and three-dimensional simulations of a single droplet dynamics rising by buoyancy with mass transfer.

INTRODUCTION

Droplets dynamics with mass transfer is encountered in several industrial processes, as for example in liquid-liquid extraction. In liquid-liquid extraction, two immiscible fluids (an aqueous phase and an organic phase) are counter-currently contacted and mixed together and the extraction process takes place at the liquid-liquid interface. Understanding the interface dynamics, droplet interaction and extractant effect on droplet

break-up and coalescence is very important as these small scale phenomena can significantly affect the overall flow and hence the extraction efficiency. High-fidelity simulation of droplets dynamics with mass transfer can play an important role in this understanding and also in the development of improved modeling terms for the multiphase flow formulation. Therefore, our goal is to develop accurate computational capabilities to simulate droplets dynamics relevant to liquid-liquid extraction.

Despite the fact that substantial improvements have been made over the last two decades in computational methods for two-phase flow with interface tracking, it is still very challenging to accurately model interfacial flow, in particular, with mass transfer. To date, only a few computational methods have been reported to model droplet dynamics with mass transfer: body-fitted grid method (Mao et al., 2001), front-tracking method (Koyonov et al, 2005 and Darmana et al., 2006), level-set method (Yang and Mao, 2005), and volume-of-fluid method (Davidson and Rudman 2002, Kroger et al. 2007, Onea et al. 2009). Among these studies only a few (Darmana et al, 2006 Yang and Mao 2005, Kroger et al. 2007, Onea et al. 2009) have modeled the discontinuity in species concentration (non-unity distribution coefficient) and described their computational approach.

In this work, we extend our own balanced-force volume tracking algorithm (Francois et al. 2006) to include species transport and diffusion and we propose a new formulation, “the global embedded interface formulation” to model the jump

¹ By acceptance of this paper, the publisher recognizes that the U.S. Government retains a nonexclusive, royalty-free license to publish or reproduce the published form of this contribution, or to allow others to do so, for U.S. Government purposes.

conditions in species concentration at the interface. We then validate our computational formulation with several test cases.

FLOW SOLVER

Here, we consider the flow to be incompressible and isothermal and governed by a single set of mass and momentum conservation equations on a fixed grid. The interface between the fluids is not explicitly tracked but is represented by the volume fraction of each fluid. The volume fractions, f , are evolved with an advection equation. Here, we consider the case of two immiscible Newtonian fluids, denoted by subscripts 1 and 2. In computational cells occupied with fluid 1, f is unity, and in cells occupied with fluid 2, f is zero. For cells containing the interface bounding fluid 1 and 2, f lies between zero and unity. The volume fractions of fluid 1 and 2 sum to unity in every computational cell.

The governing equations for the fluid flow are the equation for the advection of the volume fraction f :

$$\frac{\partial f}{\partial t} + \bar{u} \cdot \nabla f = 0 ; \quad (1)$$

and the mass and momentum conservation equations:

$$\nabla \cdot \bar{u} = 0 \quad (2)$$

$$\frac{\partial(\rho \bar{u})}{\partial t} + \nabla \cdot (\rho \bar{u} \bar{u}) = -\nabla P + \nabla \cdot (\mu(\nabla \bar{u} + \nabla^T \bar{u})) + \rho \bar{g} + \sigma \kappa \hat{n} \delta \quad (3)$$

where ρ and μ are the fluid density and viscosity, respectively, defined as

$$\rho = \rho_1 f + \rho_2 (1 - f) \quad (4)$$

$$\mu = \mu_1 f + \mu_2 (1 - f) \quad (5)$$

The expression for density in Eq. (4) results from mass conservation, whereas the expression for mixture viscosity in Eq. (5) is an approximation. The system of equation (Eq. 2-3) is solved using a pressure correction projection method as described in Francois et al. (2006) and the volume fraction advection equation (Eq. 1) is solved using the volume tracking algorithm (Rider and Kothe 1998). It consists of geometrically reconstructing piecewise linear interface planes (PLIC) to keep a sharp representation of the interface.

Modeling the surface tension force in volume tracking methods is challenging, as the continuum surface force model (CSF) of Brackbill et al. (1992) is known to generate unphysical flow (“spurious current”) near the interface. In the CSF model, the surface tension force is expressed as a localized volumetric force, $\vec{F}_{CSF} = \sigma \kappa \hat{n} \delta$, where δ is the delta function, κ is the interfacial curvature, σ is the surface tension coefficient and \hat{n} is the unit interfacial normal. Difficulties with the CSF model are due to inconsistent force balance discretization across the interface and inaccurate or non-convergent curvature estimates. To remediate the first issue, the balanced-force

algorithm of Francois et al. (2006) has been designed to ensure exact discrete force balance between surface tension forces and the resulting pressure gradients. Combined with the second-order accurate height function method (Francois et al. 2006) to estimate the interface curvature, the balanced-force volume tracking algorithm results in significant reduction of the spurious currents.

SPECIES DIFFUSION AND TRANSPORT

We consider two immiscible fluids in which a single solutal species is dissolved. Let $R_1(t)$ and $R_2(t)$ denote the disjoint regions occupied by fluid 1 and fluid 2 at time t . The governing equation for the species concentration in each fluid is the advection-diffusion conservation equation:

$$\frac{\partial C_i}{\partial t} + \nabla \cdot (C_i \bar{u}) = \nabla \cdot (D_i (\nabla C_i)), \text{ in } R_i. \quad (6)$$

At the liquid-liquid interface, we have continuity of the solute flux across the interface:

$$D_1 \frac{\partial C_1}{\partial n} = D_2 \frac{\partial C_2}{\partial n} \quad (7)$$

and at thermodynamic equilibrium, the species concentration on both sides of the interface can be discontinuous

$$\frac{C_2}{C_1} = m \quad (8)$$

where $m > 0$ a given constant is known as the distribution coefficient. It is important to observe that Eq. (6) are separate equations holding for each fluids in disjoint regions that are coupled through the interface conditions (Eq. 7 and 8).

An equivalent global model. In order to solve the species transport with the interface conditions given in Eq. (7) and (8), we first need to derive an equivalent model. Let us define

$$a(x, t) = \begin{cases} 1, & x \text{ in } R_1 \\ m, & x \text{ in } R_2 \end{cases} \quad (9)$$

and consider the problem

$$\frac{\partial a \psi}{\partial t} + \nabla \cdot (a \psi \bar{u}) = \nabla \cdot (a D (\nabla \psi)). \quad (10)$$

where $\psi(x, t)$ is defined in the entire domain and $D = D_i$ on R_i .

If ψ is a solution of (10) and we define

$$C_i = a \psi|_{R_i}, \quad i = 1, 2, \quad (11)$$

then C_i satisfies (6) and the conditions (7) and (8). Thus Eq. (10) can be viewed as a global advection-diffusion model equivalent to Eq. (6) that embeds the interface conditions implicitly within the solution. It is convenient to rewrite Eq. (10) as a coupled differential-algebraic system

$$\frac{\partial C}{\partial t} + \nabla \cdot (C\bar{u}) + \nabla \cdot \bar{\phi} = 0 \quad (12)$$

$$\bar{\phi} = -aD\nabla\psi \quad (13)$$

$$C = a\psi \quad (14)$$

for the fields ψ , C and $\bar{\phi}$. Here ψ and $\bar{\phi}$ are continuous across the interface and C is discontinuous due to the discontinuity in a at the interface.

In previous studies, the discontinuity in species concentration was treated by a transformation to make the concentration continuous across the interface (Yang and Mao (2001) used a transformation by \sqrt{m} and Kroger et al. (2007) and Onea et al (2009) a transformation by m in the gas phase), and by modifying the diffusion flux term near the interface (usually by locally modifying the diffusion coefficient). Darmana et al. (2006) introduced a volumetric source term near the interface using a delta function. Note that our approach is simpler as it is a global approach that does not need to introduce local modification as in the previous studies.

Discretization of the global model and coupling to the fluid flow solver. The diffusion solver package PEDERNAL (Carlson et al. 2009) solves the system of equation (Eq. 12-14) using a local mimetic finite-difference scheme (see Morel et al. 2001, for example). The fields ψ and C are approximated by cell-averages, and the flux $\bar{\phi}$ is approximated by normal component face-averages. Eq. (12) is discretized directly by integrating it over each computational cell. The advection term is calculated at the current time step by the flow solver and is treated as a source term. Eq. (13) is treated weakly by dotting it with test functions from the flux space and integrating. In the local formulation of the mimetic finite difference method, the fluxes can be eliminated by introducing face-based Lagrange multipliers that approximate the average of ψ on the mesh faces, which relies on the assumed continuity of ψ . The algebraic equation Eq. (14) is interpreted cell-by-cell. For a single-material cell (that is a cell contained wholly in R_1 and R_2), the value of C is either $1 \times$ or $m \times$ the value of ψ on the cell, as appropriate. For a mixed cell, the multiple of ψ is based on a volume fraction weighted combination of 1 and m . The resulting semi-discretized equations form a differential-algebraic system for C and ψ on cells and Lagrange multipliers on faces (ψ on faces) that is solved by the time integrator. The time discretization for the diffusion solver employs first and second order implicit BDF1 and BDF2 and uses the nonlinear Krylov method (Carlson and Miller 1998) to solve the resulting time step equations. The overall time step for the coupled system with the fluid flow is determined as the minimum of all the different physics-driven time steps (advection, diffusion, viscous or surface tension).

RESULTS

One-dimensional diffusion problem. To validate the species transport solver and the global model, we consider the diffusion problem in one-dimension. Initially, the concentration is constant equal to C_0 in fluid 1 ($x>0$) and in fluid 2 ($x<0$) the species concentration is zero. The analytical solution for an infinite domain with the interface located at $x=0$ is given in Crank (1975) by:

$$\frac{C_1}{C_0} = \frac{1}{1 + m\sqrt{D_2/D_1}} \left\{ 1 + m\sqrt{D_2/D_1} \operatorname{erf} \left(\frac{x}{2\sqrt{D_1 t}} \right) \right\} \quad (15)$$

$$\frac{C_2}{C_0} = \frac{m}{1 + m\sqrt{D_2/D_1}} \operatorname{erfc} \left(\frac{|x|}{2\sqrt{D_2 t}} \right) \quad (16)$$

In our simulation, the computational domain is finite with no species flux at the end points. We first consider a domain of size $[-1.5, 1.5]$ with $m=5$ and $D_2/D_1=1$ and 128 cells. The species concentration profile is plotted in Figure 1 at an early time $t=0.1$ and compared to the analytical solution at early times before the diffusion boundary layer has reached the end of the computational domain. We find very good agreement between the computational results and the analytical solution. Our computations are able to capture the jump in the species concentration values. If the interface is located on a cell edge (i.e. the volume fraction in the cell just left of the interface is 1 and in the cell just right of the interface the volume fraction is 0), the discontinuity is captured accurately and is sharp. If the interface is located within a computational cell (i.e. the volume fraction is between 0 and 1), the results show an intermediate value, i.e. the discontinuity is spread over one cell. Next, we investigate the effect of the mesh resolution on the same test case. The species concentration profiles using 32, 64, 128, 256 and 512 cells are plotted in Figure 2 at time $t=0.1$. This plot shows that our results converge to the analytical solution as the mesh is refined.

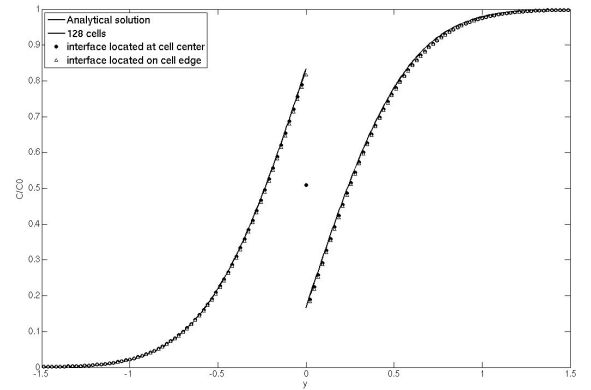


Figure 1: Effect of the interface position within the mixed cell for the one-dimensional diffusion test case with distribution coefficient $m=5$ and $D_2/D_1=1$ at time $t=0.1$ with 128 cells.

The transient solutions for the species concentration profiles are plotted in Figure 3 and compared to the analytical solution for the same test case using 128 cells and a domain of $[-3,3]$. Our computational results are able to capture the transient evolution of the species concentration and resolve the discontinuity at the interface accurately. Next, we consider a test case with a distribution coefficient $m=0.5$ and a diffusivity ratio $D_2/D_1=10$. The species concentration profile is plotted at time $t=0.1$ in Figure 4. Again, the discontinuity in the species at the interface is captured sharply if the interface is located on a cell edge and is captured over one mesh cell if the interface is located within a computational cell. With this one-dimensional diffusion test case, we have verified that our global model formulation for the species transport captures correctly the discontinuity in species concentration at the interface.

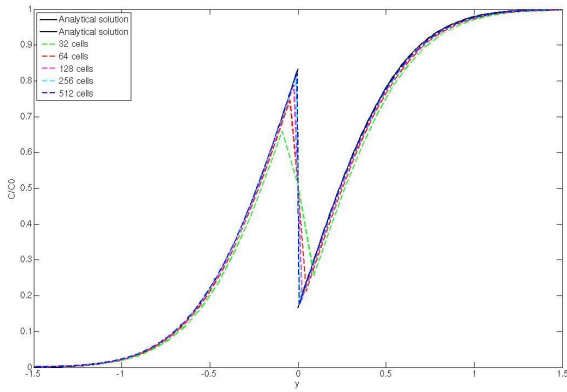


Figure 2: Mesh resolution effects for the one-dimensional diffusion test case with distribution coefficient $m=5$ and $D_2/D_1=1$ at time $t=0.1$ in a $[-1.5,1.5]$ domain. The interface is located at the cell center.

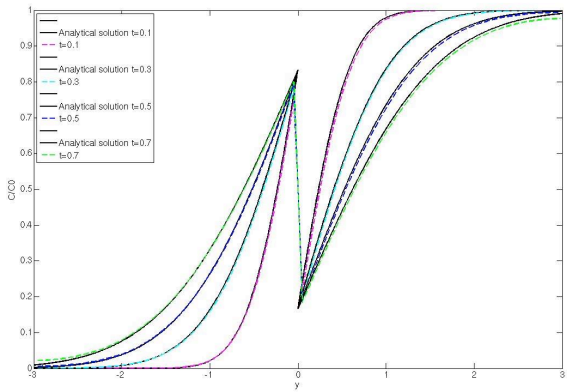


Figure 3: Transient solutions for the one-dimensional diffusion test case with distribution coefficient $m=5$ and $D_2/D_1=1$ at time $t=0.1, 0.3, 0.5$ and 0.7 . Note that the analytical solution is for an infinite domain whereas the simulation domain is finite $[-3,3]$ with no species flux at end points. The mesh size is 128 cells with the interface located at the cell center.

Two-dimensional diffusion problem. We now consider the diffusion problem of a stationary drop in two-dimensions. Initially the species concentration inside the drop (fluid 1) is 1 and the concentration outside the drop is zero. A circular drop of diameter 0.4 is centered in a square domain of length 1. We use two mesh sizes: 128×128 cells and 512×512 cells. The species concentration profiles for both meshes are plotted in Figure 5. Our results using our global method for the species transport are found in agreement with the results of Onea et al. (2009).

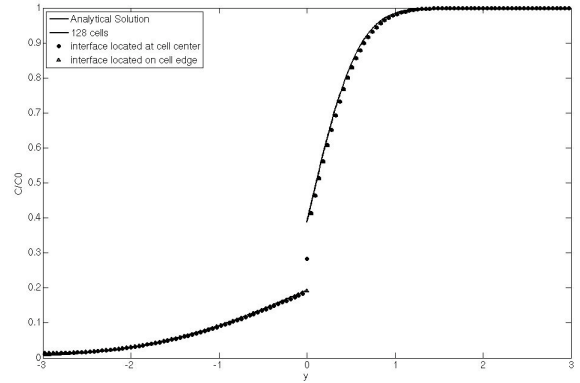


Figure 4: Effect of the interface position within the mixed cell for the one-dimensional diffusion test case with distribution coefficient $m=0.5$ and $D_2/D_1=10$ at time $t=0.1$ with 128 cells.

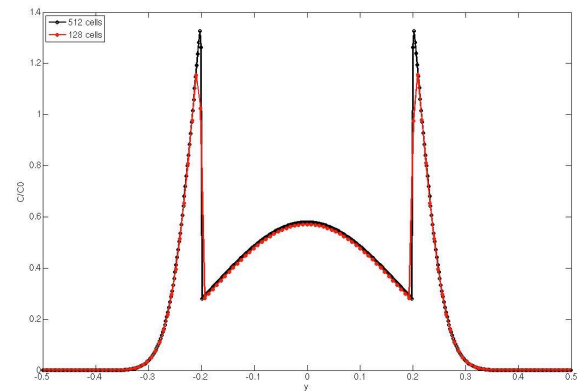


Figure 5: Effect of mesh resolution on the species concentration profile along the y -direction at $x=0$ (mid-plane) for a stationary circular drop of diameter 0.4 with distribution coefficient $m=5$ and $D_2/D_1=10$ at time $t=0.001$. The mesh sizes are 128×128 cells and 512×512 cells. Initially the concentration in the drop is 1 and 0 outside.

Coupled fluid flow and species transport problem: simulation of droplet rising by buoyancy. We perform simulations in two and three dimensions of a single droplet rising by buoyancy with single species diffusion. The droplet is initially circular in 2D (spherical in 3D) of diameter $d = 0.4$. The droplet is denoted by fluid 1 (subscript 1) and the other

fluid by fluid 2. The fluid densities are $\rho_1 = 0.001$ and $\rho_2 = 0.01$. The fluid viscosities are the same for the two fluids $\mu_1 = \mu_2 = 10^{-4}$. The surface tension coefficient is $\sigma = 0.0073$. The diffusion coefficients are the same for the two fluids $D_1 = D_2 = 0.0005$. The computational domain is rectangular of dimension $[-0.5, 0.5] \times [-1.5, 1.5]$ in 2D and $[-0.5, 0.5] \times [-1.5, 1.5]$ in 3D. The mesh size is 64×192 in 2D and $64 \times 64 \times 192$ in 3D. The gravitational acceleration, $g = 10$, is acting downward (y -direction in 2D and z -direction in 3D). We define the reference velocity U by

$$U = \sqrt{gd}. \quad (17)$$

The flow is characterized by a set of nondimensional numbers:

-Reynolds number

$$Re_1 = \frac{\rho_1 U d}{\mu_1}, \quad Re_2 = \frac{\rho_2 U d}{\mu_2}; \quad (18)$$

-Weber number

$$We_1 = \frac{\rho_1 U^2 d}{\sigma}, \quad We_2 = \frac{\rho_2 U^2 d}{\sigma}; \quad (19)$$

-Peclet number

$$Pe_1 = \frac{U d}{D_1}, \quad Pe_2 = \frac{U d}{D_2}. \quad (20)$$

Initially, the drop center is located at $y = -1.1$ and the species concentration in the drop is uniform and equal to 1 and in the background fluid the species concentration is zero. The species concentration contours and drop shape are shown in Figure 6 at time $t = 0.4, 0.8$ and 1.2 for $m = 1$ (left column) and $m = 5$ (right column). The droplet deforms to an ellipsoidal shape and reaches a constant terminal velocity (see Figure 9a) as expected for this regime ($Re_1 = 8$, $We_1 = 0.22$). A wake develops behind the droplet as illustrated in the streamlines plot in Figure 8a which affects the species concentration distribution. The result for the case $m = 1$ is in agreement with previous numerical simulation results of Mao et al. (2001) using a body-fitted method for Peclet number of order 1000. The species concentration distribution in the droplet and behind the droplet is different for the two distribution coefficients investigated, with higher concentration at the trailing edge of the droplet for the case with $m = 5$. The averaged droplet concentration and the mass transfer coefficient are plotted versus time in Figure 7.

The mass transfer coefficient is calculated as:

$$k(t) = \frac{V_d}{A_d \Delta t} (\bar{C}^{n+1} - \bar{C}^n), \quad (21)$$

with V_d the droplet volume, A_d the droplet surface area and \bar{C}^n the averaged droplet concentration at time n . The droplet surface area A_d is calculated from the PLIC interface reconstruction at every time step.

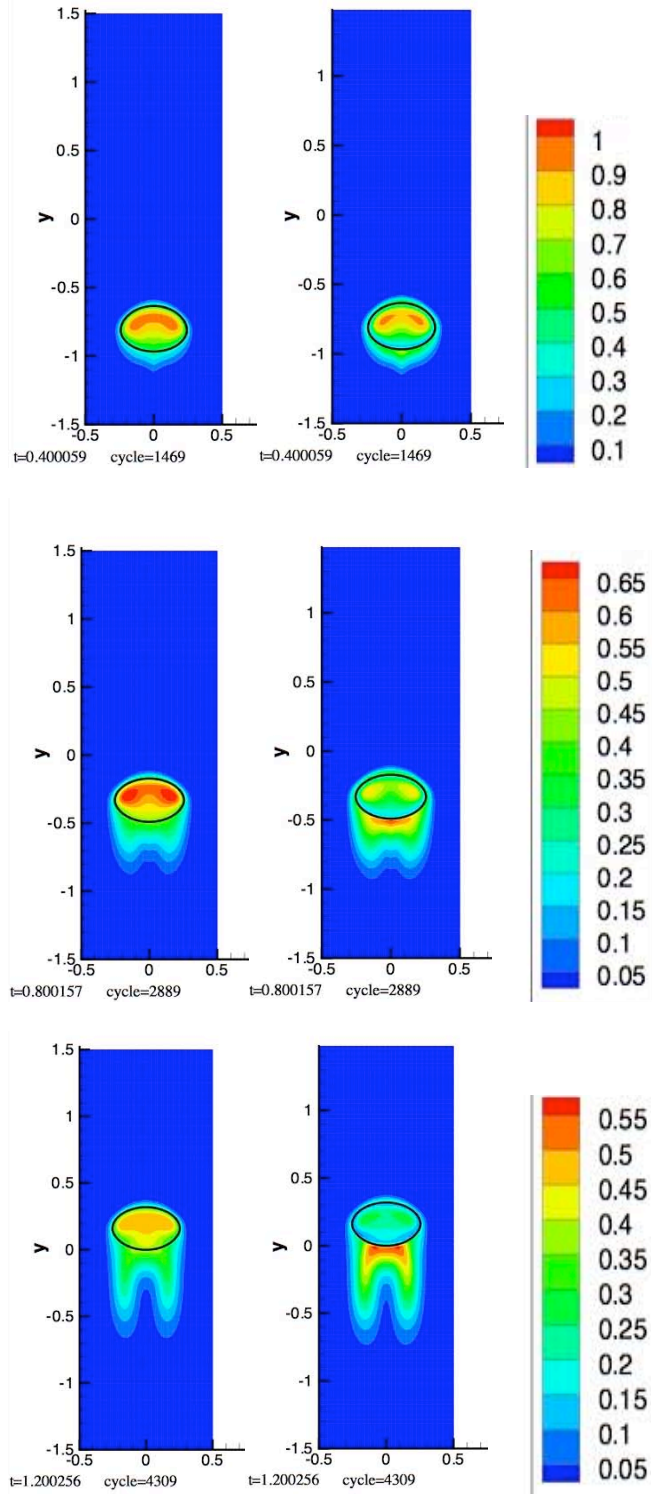
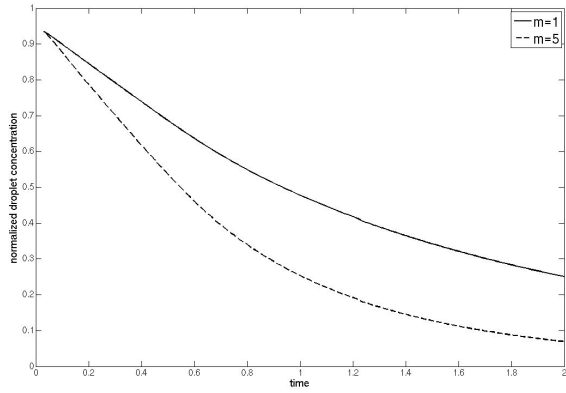
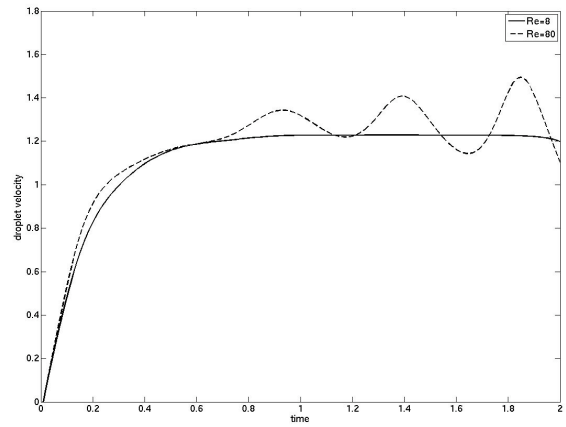


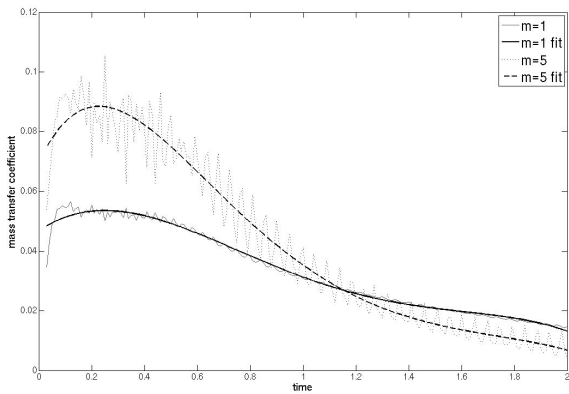
Figure 6: Species concentration contours and droplet shapes at time $t = 0.4, 0.8$, and 1.2 for $m = 1$ (left column) and $m = 5$ (right column).



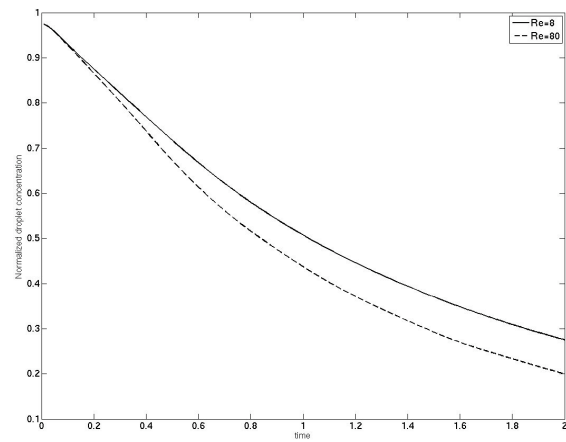
(a) Droplet concentration versus time



(a) Droplet velocity versus time

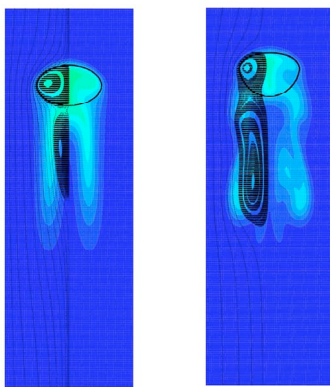


(b) Mass transfer coefficient versus time



(b) Droplet concentration versus time

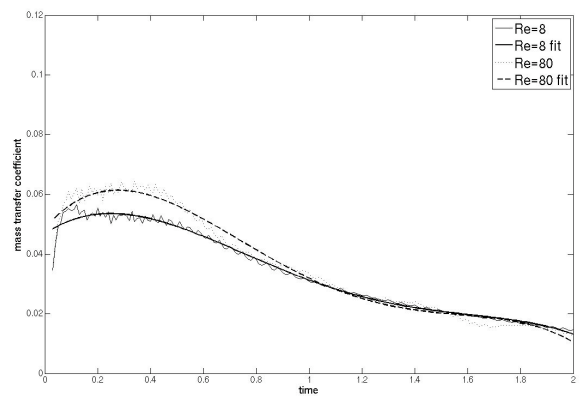
Figure 7: Effects of the distribution coefficient on (a) droplet concentration and (b) mass transfer coefficient.



(a) Re=8

(b) Re=80

Figure 8: Effects of Reynolds number on two-dimensional droplet dynamics and species concentration. Species concentration contours and droplet shape with streamtraces (on left half) in a reference frame moving with the droplet at time $t=1.8$. $We=0.22$ and $Pe=1600$.



(c) Mass transfer coefficient versus time

Figure 9: Effects of Reynolds number on (a) droplet rising velocity and (b) droplet concentration for $We=0.22$, $Pe=1600$. 2D calculation, $m=1$.

Next, we perform a simulation for a higher Reynolds number ($Re_1=80$) for same Weber and Peclet number as the previous case and for $m=1$. For this case, the droplet is in an oscillating regime as shown in the droplet velocity plot of Figure 9a. The species concentration contours for $Re=80$ are hence very different as shown in Figure 8b at time $t=1.8$ than for the case $Re=8$. The effects of the Reynolds number on the droplet velocity, droplet concentration and mass transfer coefficient versus time are shown in Figure 9. As expected, with a higher Reynolds number, the droplet concentration decreases faster than for the case with a lower Reynolds number (higher mass transfer for a higher Reynolds number). From the mass transfer coefficient one can compute the Sherwood number as

$$Sh = \frac{d}{D} k, \quad (22)$$

and correlate the Sherwood number divided by the square root of the Peclet number versus the Reynolds number. For our cases with $Re=8$ and $Re=80$, Sh/\sqrt{Pe} is found in the range of the data shown in Koyonov et al. (2005) who used a front tracking method and compared with the experimental results of Redfield and Houghton (1965).

Finally, the droplet shape and species concentration contours resulting from a three-dimensional simulation is shown in Figure 10. Note that the species concentration distribution is very different in three-dimension compared to the two dimensional simulations for the same fluid parameters. In the future, we will perform more simulation and analysis of three dimensional droplet dynamics.

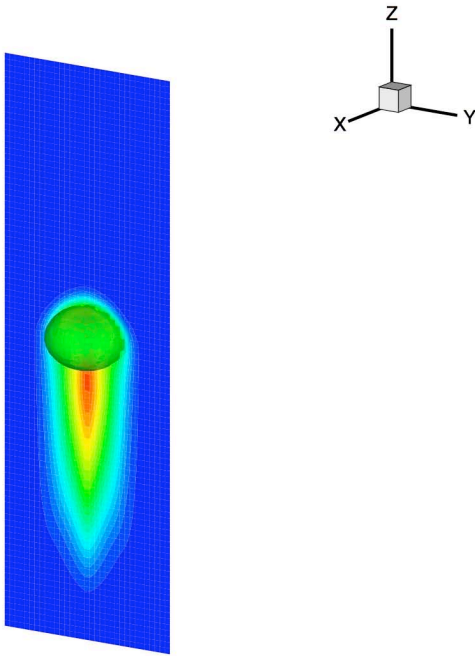


Figure 10. Droplet shape and concentration contours for 3D droplet simulation at $t=0.8$ in mid-plane. $Re=8$, $We=0.22$, $Pe=1600$, $m=1$.

CONCLUSIONS AND FUTURE WORK

We have presented a new formulation “the global embedded interface formulation” to model the discontinuity in the species concentration at an interface in thermodynamics equilibrium. The formulation is global in the sense that it does not require to locally modify the diffusion fluxes or add a volumetric source term near the interface as it was done in previous work. We have validated this new formulation for one- and two dimensional pure diffusion test cases. This embedded interface global formulation has been coupled to the balanced-force volume tracking algorithm to model interfacial flow with surface tension and mass transfer. Future work will include the development of new capabilities to model chemical reaction, soluto-capillary effects and surfactants within the balanced-force volume tracking algorithm framework.

NOMENCLATURE

1 = fluid 1 subscript
2 = fluid 2 subscript

δ = delta function
 κ = interface curvature
 μ = droplet dynamic viscosity
 ρ = droplet density
 σ = surface tension coefficient

C = species concentration
 d = droplet diameter
 D = diffusion coefficient
 f = volume fraction
 \vec{g} = gravitational acceleration
 i = species index
 k = mass transfer coefficient
 m = distribution coefficient
 \hat{n} = unit interface normal
 P = total pressure
 $Pe = Ud/D$ = Peclet number
 $Re = \rho Ud/\mu$ = Reynolds number
 $Sh = dk/D$ = Sherwood number
 t = time
 \vec{u} = fluid velocity
 U = reference velocity
 $We = \rho U^2 d/\sigma$ = Weber number

ACKNOWLEDGMENTS

This work was performed under the auspices of the National Nuclear Security Administration of the US Department of Energy at Los Alamos National Laboratory under Contract No. DE-AC52-06NA25396. This work is supported by the Nuclear Energy Advanced Modeling and Simulation Program.

REFERENCES

Brackbill J.U., Kothe D.B., Zemach C., A continuum method for modelling surface tension, *Journal of Computational Physics*, 100, 335, 1992.

Carlson N.N., Berndt M., Lally B., PEDERNAL: Numerics and code overview, Los Alamos National Laboratory, LA-UR 09-07050, 2009.

Carlson N.N., Miller K., Design and application of a gradient-weighted moving finite element code I: In one dimension, *SIAM Journal on Scientific Computing*, 19, 728-65, 1998.

Crank J., *The Mathematics of Diffusion*, Oxford Science Publications, 1975.

Darmana D., Deen N.G., Kuipers J.A.M., Detailed 3D modeling of mass transfer processes in two-phase flows with dynamic interfaces, *Chemical Engineering Technology*, 29, 1027-1033, 2006.

Davidson M.R. and Rudman M., Volume-of-Fluid calculation of heat or mass transfer across deforming interfaces in two-fluid flow, *Numerical Heat Transfer P*, 41, 291-308, 2002.

Francois M.M., Cummins S.J., Dendy E.D., Kothe D.B., Sicilian J.M, Williams M.W., A balanced-force algorithm for continuous and sharp interfacial surface tension models within a volume tracking framework, *Journal of Computational Physics*, 213, 141, 2006.

Koyonov A., Khinast J. G., Tryggvason G., Mass transfer and chemical reactions in bubble swarms with dynamics interfaces, *AIChE Journal*, 51, 2786, 2005.

Kroger M., Alke A., Bothe D., Warnecke H.-J., A VOF-based approach for the simulation of reactive mass transfer from rising bubbles, 4th International Berlin Workshop on Transport Phenomena with Moving Boundaries, Berlin, Germany, 2007.

Mao Z.-S., Li T., Chen J., Numerical simulation of steady and transient mass transfer to a single drop dominated by external resistance, *International Journal for Heat and Mass Transfer*, 44, 1235, 2001.

Morel J.E., Hall M.L., Shashkov M.J., A local support-operators diffusion discretization scheme for hexahedral meshes, *Journal of Computational Physics*, 170, 338-72, 2001.

Onea A., Worner M., Cacuci D.G, A qualitative computational study of mass transfer in upward bubble train flow through square and rectangular mini-channels, *Chemical Engineering Science*, 64, 1416-1435, 2009.

Redfield J.A., Houghton G., Mass transfer and drag coefficient for single bubbles at Reynolds number of 0.02-5000, *Chemical Engineering Science*, 20, 131-139, 1965.

Rider W. Kothe D.B., Reconstructing volume tracking, *Journal of Computational Physics*, 141, 112, 1998.

Yang C., Mao, Z.-S., Numerical simulation of interphase mass transfer with the level set approach, *Chemical Engineering Science*, 60, 2643-2660, 2005.